Coverage-dependent molecular tilt of carbon monoxide chemisorbed on Pt{110}: A combined LEED and DFT structural analysis

Sofia Karakatsani[1], Qingfeng Ge[2], Michael. J. Gladys[1,3] Georg Held[1,4] *

David A. King[1]

[1] University of Cambridge, Department of Chemistry, Lensfield Rd, Cambridge, UK

[2] Southern Illinois University, Department of Chemistry & Biochemistry, Carbondale, IL 62901, USA

[3] University of Newcastle, School of Mathematical and Physical Sciences, Callaghan, 2308, Australia

[4] University of Reading, Department of Chemistry, Whiteknights, Reading, UK

* **Corresponding address:**

University of Reading, Department of Chemistry

Whiteknights, Reading RG6 6AD UK

Email: g.held@reading.ac.uk

Abstract

The adsorption of carbon monoxide on the Pt{110} surface at coverages of 0.5 ML and 1.0 ML was investigated using quantitative low-energy electron diffraction (LEED IV) and density-functional theory (DFT). At 0.5 ML CO lifts the reconstruction of the clean surface but does not form an ordered overlayer. At the saturation coverage, 1.0 ML, a well-ordered $p(2 \times 1)$ superstructure with glide line symmetry is formed. It was confirmed that the CO molecules adsorb on top of the Pt atoms in the top-most substrate layer with the molecular axes tilted by $\pm 22^{\circ}$ with respect to the surface normal in alternating directions away from the close packed rows of Pt atoms. This is accompanied by significant lateral shifts of 0.55 Å away from the atop sites in the same direction as the tilt. The top-most substrate layer relaxes inwards by -4 % with respect to the bulk-terminated atom positions, while the consecutive layers only show minor relaxations. Despite the lack of long-range order in the 0.5 ML CO layer it was possible to determine key structural parameters by LEED IV using only the intensities of the integer-order spots. At this coverage CO also adsorbs on atop sites with the molecular axis closer to the surface normal ($< 10^{\circ}$). The average substrate relaxations in each layer are similar for both coverages and consistent with DFT calculations performed for a variety of ordered structures with coverages of 1.0 ML and 0.5 ML.

1 Introduction

Understanding in detail the complex processes involved in chemisorption and heterogeneous catalysis requires exact knowledge of the positions of substrate and adsorbate atoms. Thus, the structural analysis of surfaces of catalytically important metals is of special importance. Platinum has widespread use in heterogeneous catalysts , e.g. in the automotive three-way catalyst where it catalyzes the oxidation of uncombusted hydrocarbons and carbon monoxide [1]. In particular, adsorption on the Pt{110} surface has been the subject of various theoretical and experimental investigations in the modern surface science era because it represents a prototype for adsorbate-induced structure transformations in an ultrahigh vacuum environment (UHV) with dramatically changing reactivities depending on the structure of the substrate [2, 3, 4, 5, 6, 7, 8, 9, 10, 11, 12, 13, 14, 15, 16, 17, 18, 19, 20, 21, 22, 23, 24, 25, 26, 27, 28, 29, 30, 31, 32, 33]. The clean Pt{110} surface exhibits a $p(1 \times 2)$ "missing row" reconstructed phase, where every second row in the [001] direction is missing [4, 18, 26]. Exposure to CO at temperatures above 250 K lifts the reconstruction, forming a $p(2 \times 1)$ superstructure at saturation or a disordered "(1×1)" phase at lower coverage [8, 9, 31].

Missing spots in the low-energy electron diffraction (LEED) pattern of the $p(2 \times 1)$ phase indicate glide-line symmetry [3]. King et al. proposed a tilted geometry with opposite tilt directions for the two molecules in this unit cell (1 molecule per surface Pt atom) [5, 6, 10, 11, 12]. This was the first CO adsorption system for which a tilted geometry was proposed. The model involves adsorption on atop positions and explains the tilting as a way to avoid excessively close packing when the molecules are adsorbed at neighboring sites along the atomic ridges. The magnitude and orientation of the tilt angle has been studied with several techniques. On the basis of angle-resolved ultra-violent photoemission spectra (ARUPS) it was concluded that the CO molecular axis is tilted between 20° and 26° away from the surface normal with an azimuthal orientation between the [001] [13]

and [1$\bar{1}$2] directions [10]. More recent X-ray photoelectron diffraction (XPD) measurements determined a tilt angle of 22° along the [001] azimuthal direction [29]. In addition, there is evidence from XPS and IR spectroscopy that the molecules adsorb on atop sites [15, 29, 16, 21, 27]. Other structural parameters for CO adsorption have been studied theoretically using density functional theory (DFT) [28, 30, 32], but there is no quantitative experimental data for structural parameters such as bond lengths and substrate reconstruction in this adsorption system.

When the Pt{110} surface is covered with a CO coverage greater than 0.2 ML the missing-row reconstruction is gradually lifted at room temperature [7, 22, 23, 31]. This changes dramatically the surface reactivity, e.g. for dissociation of oxygen molecules, and thus gives rise to spatial and temporal oscillatory phenomena in the CO oxidation [19, 24]. At around 0.5 ML the superstructure spots originating from the reconstruction have disappeared but no new adsorbate-induced superstructure spots are observed in the LEED pattern at this coverage [8, 9, 29]. This poses a challenge to quantitative LEED IV analysis, however recent studies have shown that adsorbate-related contributions to the intensities of integer-order diffraction beams are almost independent of the state of long-range order in the adsorbate layer [34, 35, 36]. Thus, an accurate and reliable analysis of lattice-gas disordered adsorbate layers can be achieved by using integral-order LEED beams only, provided the data set is large enough. In this paper, we present the results of a complete structural analysis of CO on the unreconstructed Pt{110} surface at full saturation (1.0 ML) and 0.5 ML coverage using LEED IV and *ab initio* density functional theory. The experimental results are in good agreement with the model calculations.

2 Details of Experiment and Calculations

2.1 LEED Experiment

LEED intensity measurements were carried out in a conventional stainless steel ultra-high vacuum (UHV) chamber, operating at a base pressure of 5×10^{-11} mbar. The system was equipped with a four-grid Omicron reverse-view LEED optics and is described in detail elsewhere [37]. The Pt{110} crystal cleaning consisted of several cycles of argon-ion bombardment at 300 K followed by annealing to 1200 K, exposure to oxygen (1×10^{-7} mbar) in the temperature range 400 to 1100 K to remove any residual carbon, and flash annealing to 1000 K to remove oxygen. This procedure produces a sharp $p(1 \times 2)$ diffraction pattern with low background intensities. The surface cleanliness was checked by oxygen temperature programmed desorption (TPD). Reproducible spectra in agreement with those in the literature [38] are only achieved for clean surfaces. Several different preparations for the CO layers were tested, varying the crystal temperature and CO exposure, in order to improve the quality of the LEED pattern. The (1×1) phase studied here was produced by background CO exposure to 20 L (1L = 10^{-6} Torr·s) at 400 K, Figure 1.a. Further exposure to 120 L at 300 K led to the 1 ML $p(2 \times 1)$ superstructure with missing spots, Figure 1.b.

The LEED measurements were carried out at a sample temperature of 100 K to reduce background intensity caused by thermal vibrations. The incident electron beam was tilted by about 5° within the [001] symmetry plane of the {110} surface. A commercial video LEED system was used to record the diffraction pattern in an energy range from 50 eV to 300 eV in steps of 1 eV. No beam damage was observed due to fast data acquisition (less than 10 min per IV run). Our own spot-tracking program, MKIV, was used for the extraction of the IV curves of all visible beams simultaneously [39]. The IV curves were further processed by averaging the beams, which are symmetry-

equivalent with respect to the (001) plane, and by Fourier smoothing to reduce experimental noise. Since the data were recorded not exactly within the symmetry plane, the IV curves of nominally symmetry equivalent beams were slightly different. Even averaging does not compensate these differences. Therefore both angles of incidence were treated as additional fit parameters. For the $p(2 \times 1)$-CO surface, a total of 27 beams were extracted (14 independent beams); for the disordered 0.5 ML structure 16 beams were recorded (10 independent beams).

2.2 LEED Calculations

The model calculations for the LEED structure determination were performed with our "CLEED" program package [40], which is an implementation of fully dynamical scattering theory based on algorithms described by Pendry [41] and Van Hove and Tong [42].

LEED intensities were calculated for electron energies between 50 and 200 eV in steps of 4 eV. Relativistic scattering phase shifts for Pt and non-relativistic phase shifts for C and O were calculated with the program package provided by Barbieri and Van Hove [43]. All phase shifts were used up to a maximum angular momentum quantum number, l_{max}, of 8. The imaginary and real parts of the optical potential, V_i and V_r, were fixed at -4 eV and -15 eV for both the saturated coverage structure and the disordered 0.5 ML structure. For the structure optimization and the determination of the angles of incidence the downhill simplex method [44, 45] was used. The convergence criterion was that the R factor values change by less than 1×10^{-4}. To quantify the agreement between experimental and theoretical IV curves in the geometry optimization, Pendry's R-factor, R_P, was used [46]. The R_P value is the optimum achieved by shifting the energy axes of experimental and theoretical IV curves with respect to each other. To some extent this shift compensates small errors in the real part of the optical potential used in the LEED calculations, but

the effect is slightly different. Therefore, V_r was re-adjusted in the final stage of the structure optimization. The error bars for each structural parameter Δp were calculated automatically by the search program following Pendry's RR factor method [46]. The error margin $\pm\Delta p$ for a given parameter is the range around the best fit parameter value, p_0, for which Pendry's R factor stays below $R(p_0) \cdot (1 + RR)$. RR is defined as $\sqrt{8|V_i|/\Delta E}$, with ΔE being the cumulative energy overlap between experimental and calculated IV curves. Assuming a quadratic behavior of the R factor in the proximity of p_0, i.e. $R(p_1) - R(p_0) = \alpha \cdot (p_1 - p_0)^2$, Δp can be estimated using the following equation [47]:

$$\Delta p = |p_1 - p_0| \cdot \sqrt{\frac{RR \cdot R(p_0)}{R(p_1) - R(p_0)}}$$

A distance of 0.1 Å between the minimum p_0 and the test value p_1 was used initially. If the so-found value of Δp was not within $\pm 25\%$ of $|p_1 - p_0|$ the calculation was iterated using $p_1^{new} = p_0 + \Delta p^{old}$ until the test value was sufficiently close to the error limit (within 25% of Δp). In case of a quadratic behavior Δp is directly related to the curvature of the R factor curve near the minimum through $\alpha = RR \cdot R(p_0)/(\Delta p)^2$. For the coordinates of the oxygen and carbon atoms the R factor curves showed strong asymmetries. In these cases, the error ranges were determined directly through R_P vs p plots (see below). The cumulative energy overlaps of 1550 eV and 980 eV for the two overlayers in the present study lead to RR values of 14% and 18%, respectively.

2.3 DFT calculations

Periodic DFT calculations including spin-polarization have been carried out using the VASP code [48]. The electron-ion interactions were described by projector augmented wave potentials [49] and the valence electrons were treated explicitly with a plane-wave cutoff energy of 400 eV. The non-local exchange-correlation energy was calculated with

the PW91 functional [50]. The Pt{110} surfaces were simulated with a slab containing 5 layers and a vacuum gap of 12 Å. The surface Brillouin zone of the $p(2 \times 1)$ surface unit cell was sampled with the k-point grids of $(4 \times 6 \times 1)$. The bottom layers were fixed at the relaxed bulk positions whereas the top layers together with the adsorbed CO molecules were allowed to optimize according to the calculated Hellman-Feynman forces by using the quasi-Newton or conjugate-gradient method, as implemented in VASP. Gaussian smearing with a width of 0.1 eV was employed to improve the convergence of the electronic self-consistent cycles. A calculation was considered as converged when the changes in energy and forces were less than 1.0×10^{-6} eV and 0.05 eV/Å, respectively.

3 LEED results

3.1 $p(2 \times 1)$ phase of 1 ML CO on Pt{110}

Exposure of the $p(1 \times 2)$ phase of Pt{110} to 120 L of CO at 300 K lifts the missing row reconstruction of the clean surface and leads to the formation of an ordered $p(2 \times 1)$ superstructure. Systematic absences of the $(\pm(h + \frac{1}{2}), 0)$ beams (h is an integer number) indicate glide line symmetry along the $[1\bar{1}0]$ direction. Since the $p(2 \times 1)$ superstructure occurs at 1 ML coverage, each $p(2 \times 1)$ unit cell is occupied by two CO molecules. The LEED structure search started by placing the molecules on each of the high symmetry sites, (i.e. atop sites and bridge sites). There are two possible non equivalent bridge sites, one along the close packed [110] (short bridge site) and the other along the [100] direction (long bridge site), as shown in Figure 2. The initial geometries for each of the structures had CO in a tilted orientation alternating in a zig-zag fashion to avoid excessive close packing (see Figure 2). This produces the glide plane symmetry in the observed LEED pattern in Figure 1.b. For the substrate a bulk-terminated geometry was assumed, and the C, O and the first and second layer Pt atoms were allowed to move vertically and laterally, while the third layer Pt atoms could relax only in the vertical direction. Distortions in

the first Pt layers and the CO molecules were coupled in accordance with the glide-line symmetry. **In addition, the angle of incidence was optimized in parallel with the structural optimization, which increased the number of search parameters by two. In total, 15 parameters were optimized.** The lowest R_P-factor values for each test geometry are shown in Table 1. From this table, the two non-equivalent bridge adsorption sites can be disregarded, since they are well outside the 14% error bar of the atop model.

The next step in the structure determination was the refinement of non-geometric parameters. By manually varying the optical potential and performing a full calculation for each value (with all the other parameters the same as the initial trial geometry) the R_P-factor could be reduced to 0.277 for a value of -15 eV. The vibrational amplitudes of the C, O and Pt atoms (up to the fourth layer) were optimized in a similar fashion. R_P decreased to 0.242 for a structure with rms displacements of 0.195 Å for O, 0.140 Å for C, 0.125 Å for first layer Pt atoms, 0.07 Å for second layer Pt atoms, 0.06 Å for third layer Pt atoms and 0.03 Å for the bulk Pt atoms. The highest improvement in the vibrational amplitude refinement came from the first layer Pt atoms. This can be expected since Pt atoms are stronger scatterers than the C and O atoms. The best-fit structure found by this search is depicted in Figure 3; the geometrical parameters for this structure are listed in Table 2. A comparison between the experimental and theoretical IV curves for this structure is shown in Figure 4.

3.2 Disordered layer of CO at 0.5 ML coverage

A CO exposure of about 20 L at 400 K is enough to lift the $p(1 \times 2)$ missing row reconstruction of the clean Pt{110} surface completely. As a result, a (1×1) LEED pattern is observed, as shown in Figure 1.a. The absence of fractional order diffraction spots indicates that no long range ordering of the CO layer occurs at this coverage. By comparing the areas under the TPD spectra for saturation coverage and the so-prepared disordered layer

the coverage was determined to be 0.54 ML. Additional information from XPS [15, 29, 32] and IR spectroscopy [27] indicates that only one type of adsorption site, most likely atop, is occupied. As shown earlier by Held et al. [35, 36], a LEED IV analysis of a simple adsorption system can be performed reliably by only using integral order LEED beams. In order to model the disordered layer at 0.5 ML, LEED IV calculations were performed using long-range ordered superstructures with three different unit cells, $c(2 \times 2)$, $p(2 \times 1)$ and $p(1 \times 2)$, each of which have a local coverage of 0.5 ML. In the model calculations the C and O atoms were placed on atop and and short bridge adsorption sites, as shown in Figure 5.a-c and d-f, respectively.

As described earlier for the 1.0 ML structure, the aim of the first step in the structural analysis was to rule out some of the initial trial models. In this step the positions of the C, O, and the first two Pt layer atoms were optimized laterally and vertically, while the third layer Pt atoms were only relaxed vertically. The lower-lying substrate layers were considered bulk-like. No symmetry was taken into account. Although there is clear spectroscopic evidence that the CO adsorption site is the same for saturation and lower coverages [27, 29, 32], both atop and bridge sites were tested in order to determine the level of sensitivity of the LEED analysis towards the adsorption site. The angle of incidence was included in the search at this stage since the LEED data were recorded at slightly off-normal-incidence conditions. In total, 22 parameters were optimized in the search. The R_P values obtained for atop adsorption in the three long-range order models were almost identical; 0.222, 0.222 and 0.220, respectively, for the $c(2 \times 2)$, $p(2 \times 1)$ and $p(1 \times 2)$ structures (see Table 1). This indicates that lateral multiple scattering between the molecules plays a minor role and the details of the long-range order (or lack thereof) in the adsorbate layer do not significantly affect the LEED IV curves of the integer order beams. The corresponding R-factors for the short bridge site are 0.346, 0.311 and 0.304; these are well outside the error margins of the atop structures and can therefore be disregarded.

By optimizing the **real part of the optical potential (optimum value 10 eV)** the R-factors for the atop structures could be significantly reduced to 0.183, 0.170 and 0.181, respectively. Note that these values are much lower than for the 1.0 ML $p(2\times1)$ structure because only integer order beams are compared. A comparison between the experimental and theoretical IV curves of these three models is presented in Figure 7. The structure parameters are listed in Tables 3 and 4.

4 DFT results

The adsorption of CO on the Pt{110}-(1×1) and reconstructed Pt{110}-$p(1\times2)$ surfaces has been subject to an earlier DFT study using the CASTEP code [28]. The results for CO on the (1×1) surface showed that the atop and short bridge sites are energetically almost degenerate. In the present study, we reexamined the previous results and focused on the atop and short bridge sites only. As the LEED analysis clearly shows that atop adsorption sites are assumed in the real system (see above), we concentrate our discussion of structures on these geometries and refer to Table 5 for additional details of the bridge geometries. Using the VASP code, the present calculations produced adsorption energies of 2.154 eV for atop sites and 2.074 eV for bridge sites at a CO coverage of 0.5 ML with a $p(2 \times 1)$ supercell (see Table 5, geometry b). These energies are comparable to those calculated with CASTEP. The geometries of the relaxed structures are also similar to the previous results. In the most stable atop site, CO is slightly tilted, with the C-O bond axis 6° off the surface normal. Other structural parameters and vibration frequencies are summarized in Table 5. The C-O stretch frequency calculated for atop adsorption, 2054 cm^{-1}, clearly agrees better than the bridge structure with the experimental data by Sharma et al., who report a values around 2070 cm^{-1} for intermediate coverages at 300 K [27]. **Although DFT in general appears to underestimate the energy difference between atop and hollow/bridge adsorption sites on Pt surfaces**

[51], it correctly reproduces the bond properties for these adsorption sites.

As the coverage is increased to 1.0 ML, the adsorbed CO molecules form a $p(2 \times 1)$ overlayer structure, with the C-O molecular axes being tilted alternately towards opposite sides of the close-packed Pt rows (see Figure 2). Again, there are stable adsorption geometries for CO on both atop and bridge sites with adsorption energies of 1.921 eV and 1.853 eV, respectively. In the atop adsorption configuration, the C-O bond is tilted from the surface normal by 19°. The adsorbed CO also causes a lateral shift in the binding Pt atoms of 0.07 Å in the [001] direction and a contraction of the first-to-second layer distance, d(1-2), by -7 % with respect to the bulk value (d(1-2) = 1.31 Å vs d(bulk) = 1.41 Å). For bridge-bonded CO, the C-O bond is tilted 18° off the surface normal. Other structural parameters, as well as C-O and C-Pt stretching frequencies, are summarized in Table 5.a. Again, the symmetric C-O stretch frequency for atop adsorption, 2073 cm^{-1}, agrees well with the experimental value of 2094 cm^{-1} for saturation at 300 K [27] (note, the asymmetric stretch mode is not observed due to symmetry selection rules).

In order to eliminate systematic errors as far as possible, additional molecular arrangements for a CO coverage of 0.5 ML on the unreconstructed Pt{110} surface, which had not been considered previously. All arrangements were studied within the same $p(2 \times 2)$ supercell, which accommodates all molecular arrangements that were used in the LEED IV analysis: $p(2 \times 1)$-CO (Figure 5.a,d; Table 5.c), $c(2 \times 2)$-CO (Figure 5.b,e; Table 5.d), and $p(1 \times 2)$-CO (Figure 5.c,f; Table 5.e). In addition, a $p(2 \times 2)$-2CO geometry was tested, which has the same adsorption sites as the $p(1 \times 2)$-CO model, however the molecules were allowed a further degree of relaxation by tilting in opposite directions, similar to the 1 ML structure (Table 5.f), and a $p(2 \times 2)$-CO arrangement with a local coverage of 0.25 ML (Table 5.g).

The calculated adsorption energies for the $p(2 \times 1)$-CO geometries within the (2×2) supercell are 2.088 eV and 2.044 eV for atop and bridge sites, respectively. They are slightly different from those calculated within the $p(2 \times 1)$ supercell (Table 5.b), by up to

0.064 eV, which gives an indication of the systematic errors involved in comparing results from different supercells. The geometrical parameters, however, are practically identical. In fact, the C-O and C-Pt bond lengths in all 0.5 ML structures only show very small differences of less than 0.01 Å. The only significant differences are in the relaxation of the first Pt layer and the greater tilt angle in the $p(2 \times 2)$-2CO geometry (Table 5.f), where the CO molecules occupy nearest neighbor sites and are allowed to tilt in opposite directions. It should be noted that the latter structure and the $p(1 \times 2)$-CO arrangement are clearly less favored in terms of adsorption energy than the structures where nearest neighbor sites are avoided. For all structures we find very similar adsorption energies for bridge and atop sites, typically within less than 0.05 eV. In addition, the very small energy difference of less than 0.05 eV between the $p(2 \times 1)$-CO and the $c(2 \times 2)$-CO arrangements may explain the lack of long-range order that has been observed experimentally for a CO coverage around 0.5 ML.

5 Discussion

At a coverage greater than 0.2 ML CO gradually lifts the $p(1 \times 2)$ missing row reconstruction of the clean Pt{110} surface and, thus, creates a substrate with a structure very different from the uncovered surface. When the surface is saturated with 1.0 ML CO a long range ordered $p(2 \times 1)$-(2CO) superstructure is formed with glide-line symmetry that leads to systematic extinctions in the LEED pattern [3, 5, 6, 8, 9, 11]. For coverages well below saturation, no long-range ordered superstructures are observed, which poses a problem for conventional LEED IV structure determination as only the intensities of integer order spots can be used. **In order to determine the key structural features of the disordered layer at 0.5 ML, three independent LEED IV analyses were carried using long-range ordered model structures with different periodicities,** $c(2 \times 2)$**,** $p(2 \times 1)$**, and** $p(1 \times 2)$ **(see Figure 5) but a common local coverage**

of 0.5 ML. Our DFT modeling clearly shows that different locally ordered arrangements lead to very similar adsorption energies and are, therefore, expected in the disordered layer at 0.5 ML. On the other hand, lateral multiple scattering paths between weak scatterers, such as C and O, only make a small contribution to the overall signal. Therefore, the long-range periodicity has only little effect on the IV curves of integer-order spots as long as the local adsorption geometries are identical [35]. As far as the local environment of the CO molecule is concerned, the key geometrical parameters extracted from the three analyses show remarkable agreement, as seen in Table 3, and an averaged local structure for CO in the disordered layer can be extracted, the parameters of which are listed in Table 4.

The LEED IV analysis clearly shows that CO adsorbs near atop sites in an almost upright orientation, whereas the DFT-calculated adsoprtion energies do not allow a discrimination between atop and bridge sites. The average tilt found in the structure determination is 9°. With a relatively small data set it is important to look at the significance of these parameters very carefully. The error ranges of the lateral coordinates of the oxygen atom are quite asymmetric around the R-factor minimum for all three 0.5 ML models tested. This is illustrated for the $p(2 \times 1)$-CO structure in Figure 8.b, where the R_P factor is plotted vs coordinate displacements from the best fit geometry. The error margin is the range of coordinate values, for which R_P is below $R_{min} \cdot (1 + RR)$. For the lateral coordinates this leads to error bars between 0.4 and 0.8 Å, with values for y typically 50% greater than for x. The diagram in Figure 8.c shows the error range of the lateral displacements between the carbon and oxygen atoms for each geometry model. [1] The +/-asymmetry around the R-factor minimum leads to error ranges which are centered very closely to the

[1] Note, the error of relative distances between atoms is the larger error of the two coordinates involved since a diffraction experiment probes interatomic distances and not absolute coordinates. The error boundaries in the two-dimensional plot were interpolated between the one-dimensional boundaries using elliptical splines.

lateral position of the carbon atom, at (0,0) in Figure 8.c, for all 0.5 ML structures. Therefore, an upright CO orientation is within 2° of the center of the error range with an uncertainty between 15° and 20°. This agrees well with the forward-focussing cone close to the surface normal measured in the XPD experiments by Nowicky et al. [29] and with the tilt angles derived from the DFT calculations, between 2° and 6°, see Table 5. There is almost perfect agreement in the C-O bond length, 1.11 ± 0.07 Å, whereas there is slightly more scatter in the values for the Pt-C bond length, from 1.79 to 1.85 Å, and the displacement of the carbon atom from the atop site towards the long bridge site ([001] direction), on average 0.34 Å. The latter is just outside the error bar of 0.3 Å. The scatter in the inter-layer spacings is less than 0.04 Å, with average values of d(1-2) = 1.30 Å, d(2-3) = 1.40 Å, and d(3-4) = 1.41 Å (see Table 4), corresponding to contractions/expansions of -6 %, $+1$ %, and $+2$ % with respect to the bulk inter-layer spacing of 1.385 Å. The error margins associated with these parameters, 0.11-0.12 Å, are larger than the deviations from the bulk positions. It must be noted, however, that Pendry's error estimate, although standard procedure, must be considered as somewhat too pessimistic [52], therefore at least the contraction of d(1-2) is likely to be significant. The corresponding values from the relaxed DFT structures with CO on atop sites are generally somewhat higher but deviate from the average experimental values by less than 0.05 Å.

A comparison of the substrate relaxation with the reconstructed clean surface is not straight forward since the second layer atoms have a different coordination, which leads to a very strong contraction of d(1-2) – experimental and calculated values range between -16 % and -21 % [18, 28, 30] – whereas d(2-3) and d(3-4) are close to the bulk inter-layer distances. In each of the 0.5 ML structures only half of the first layer Pt atoms form bonds with CO molecules. As a consequence, significant height differences and lateral shifts

are determined between these inequivalent atoms for all layers. These depend, however, much on the surface periodicity assumed in the model calculations. Therefore, no firm conclusions about the details of local Pt reconstructions can be drawn, which is a direct consequence of the lack of long-range order.

The C-O and Pt-C bond lengths determined for the 1.0 ML $p(2 \times 1)$-(2CO) superstructure are very similar to those for 0.5 ML: 1.10 Å vs 1.11 Å and 1.85 Å vs 1.83 Å, respectively. The fact that the Pt-C bond is significantly shorter than the sum of the covalent radii, 2.05 Å, indicates a strong covalent character of the substrate bond with significant net charge transfer between the adsorbate and the Pt surface. The first interlayer distance of the surface covered by 1.0 ML CO, d(1-2) = 1.33 Å, is larger than for 0.5 ML, which can also be explained by more charge transferred into the substrate at the higher coverage. **The comparison between Figures 8.a and b shows that the error margins for the lateral parameters are generally smaller than for the 0.5 ML structures, which is due to the larger data set (1550 eV vs 980 eV). In some cases the difference is up to a factor 2 (see Tables 2 and 3).**

At 1.0 ML CO molecules occupy nearest neighbor atop sites along the close-packed rows of Pt atoms. Lateral repulsion is relieved by alternating tilts of the molecular axes by $\pm 22°$ and larger lateral shifts, $\Delta x = \pm 0.55$ Å, away from the atop side. The large tilt angle is the most apparent difference between the high and low coverage structures and is in excellent agreement with earlier XPD and ARUPS results for this layer (22° [29]; 20° [13]; 26° [11]) and our DFT results (19°). **The two-dimensional plot of error ranges in Figure 8.c shows that an upright CO orientation can be firmly excluded on the basis of the LEED IV analysis. The range of possible Θ(CO) values for the $p(2 \times 1)$-(2CO) structure is between 14° and 27°. There is very little overlap the error range only with one 0.5 ML model, $c(2 \times 2)$-(CO).** The tilted arrangement appears to be caused only by lateral repulsion between the CO molecules. Comparing the calculated adsorption energies for the $p(2 \times 1)$-(2CO) (1.0 ML)

and $p(2\times1)$-CO (0.5 ML) structures in Table 5.a and b shows that the repulsion between molecules on nearest neighbor sites lowers the adsorption energy by about 0.2 eV per molecule. The repulsion between next nearest neighbor sites (along the [001] direction), on the other hand, is negligible as the comparison between the $p(2\times1)$-CO and $c(2\times2)$-CO or $p(2\times2)$-CO structures shows (Table 5.c,d,g). The calculated adsorption energies for these three structures are almost identical.

6 Summary and Conclusions

The stable $p(1\times2)$ missing row reconstruction of the clean Pt{110} surface is lifted by the adsorption of CO at coverages greater than 0.2 ML. At the saturation coverage of 1.0 ML an ordered $p(2\times1)$-(2CO) overlayer with glide-line symmetry is formed on the (1×1)-like substrate. At lower coverages around 0.5 ML no long-range order is observed.

Full LEED IV analyses were performed for the ordered overlayer at 1.0 ML coverage and the disordered layer at 0.5 ML, using only integer-order beams for the latter structure. It was found that CO adsorbs near atop sites in both cases while differences were observed regarding the orientation of the molecules and the substrate relaxation. At 0.5 ML the CO molecules are almost upright, while the molecular axis is tilted by $\pm22^\circ$ at 1.0 ML, accompanied by significant shifts of ±0.55 Å of the C atom with respect to the atop site. The Pt-C and C-O bond lengths were determined as 1.83/1.85 Å and 1.11/1.10 Å respectively for 0.5/1.0 ML. The first-to-second Pt layer distance, d(1-2), is compressed by -4/-6 % with respect to the bulk inter-layer distance, while the second to third inter-layer distances show small expansions. All geometrical parameters are in good agreement with DFT calculations.

It was possible to determine the key structural parameters of the 0.5 ML overlayer despite the lack of long-range order by using only the intensities of the integer-order spots and modeling the surface as an ordered superstructure. The precision of the structure

analysis is generally less, but still at a level comparable the ordered 1.0 ML structure, although the data set is significantly reduced. Only the details of the relaxation of individual substrate atoms remain ambiguous, which is due to the nature of the disordered surface.

Acknowledgements

This work was supported by the Engineering and Physical Sciences Research Council (EPSRC). QG acknowledges support from the US DOE, Basic Energy Sciences grant DE-FG02-05ER46231.

References

[1] I. Chorkendorff and J. W. Niemantsverdriet, *Concepts of Modern Catalysis and Kinetics*, Wiley–VCH, Weinheim (2003).

[2] H. P. Bonzel and R. Ku, J. Vac. Sci. Technol. **9** (1972) 663.

[3] R. Lambert, Surface Sci. **49** (1975) 325.

[4] D. Adams, H. Nielsen, M. Van Hove and A. Ignatiev, Surf. Sci. **104** (1981) 47.

[5] S. R. Bare, P. Hofmann and D. A. King, Vacuum **31** (1981) 463.

[6] S. R. Bare, K. Griffiths, P. Hofmann, D. A. King, G. L. Nyberg and N. Richardson, Surf. Sci. **120** (1982) 367.

[7] S. Ferrer and H. P. Bonzel, Surf. Sci. **119** (1982) 234.

[8] T. Jackman, J. Davies, D. Jackson, P. Norton and W. Unertl, J. Phys. C: Sol. State Phys. **15** (1982) L99.

[9] T. Jackman, J. Davies, D. Jackson, W. Unertl and P. Norton, Surf. Sci. **120** (1982) 389.

[10] P. Hofmann, S. R. Bare and D. A. Richardson, N. V. King, Solid State Comm. **42** (1982) 645.

[11] P. Hofmann, S. R. Bare and D. A. King, Physica Scripta **T4** (1983) 118.

[12] S. R. Bare, P. Hofmann and D. A. King, Surf. Sci. **144** (1984) 347.

[13] D. Rieger, R. Schnell and W. Steinmann, Surf. Sci. **143** (1984) 157.

[14] C. W. Bauschlicher, Chem. Phys. Lett. **115** (1985) 535.

[15] N. Freyer, M. Kiskinova, G. Pirug and H. P. Bonzel, Applied Physics A **39** (1986) 209.

[16] B. Hayden, A. Robinson and P. Tucker, Surf. Sci. **192** (1987) 163.

[17] K. Dückers, K. Prince, H. Bonzel, V. Chab and K. Horn, Phys. Rev. B **36** (1987) 6292.

[18] P. Fery, W. Moritz and D. Wolf, Phys. Rev. B **38** (1988) 7275.

[19] R. Imbihl, S. Ladas and G. Ertl, Surf. Sci. Lett. **206** (1988) L903.

[20] R. Ducros and J. Fusy, Surf. Sci. Lett. **207** (1988) L943.

[21] A. Robinson, B. Hayden and P. Tucker, Vacuum **38** (1988) 357.

[22] T. Gritsch, D. Coulman, R. J. Behm and G. Ertl, Phys. Rev. Lett. **63** (1989) 1086.

[23] J. Wintterlin and R. Behm, *Scanning Tunneling Microscopy I*, Vol. 20 of *Springer Series in Solid–State Sciences*, Springer, Heidelberg, 1. ed. (1992).

[24] G. Ertl, Surf. Sci. **299-300** (1994) 742.

[25] S. Schwegmann, W. Tappe and U. Korte, Surf. Sci. **334** (1995) 55.

[26] S. Speller, J. Kuntze, T. Rauch, J. Bommermann, M. Huck, M. Aschoff and W. Heiland, Surf. Sci. **366** (1996) 251.

[27] R. Sharma, W. Brown and D. King, Surf. Sci. **414** (1998) 68.

[28] Q. Ge and D. King, J. Chem. Phys. **111** (1999) 9461.

[29] M. Nowicki, A. Emundts, G. Pirug and H. Bonzel, Surf. Sci. **478** (2001) 180.

[30] S. Jenkins, M. Petersen and D. King, Surf. Sci. **494** (2001) 159.

[31] P. Thostrup, E. Kruse, T. Vestergaard, E. Lægsgaard and F. J. Besenbacher, J. Chem. Phys. **118** (2003) 3724.

[32] M. J. Gladys, O. R. Inderwildi, S. Karakatsani, V. Fiorin and G. Held, J. Phys. Chem. C **112** (2008) 6422 .

[33] A. Shavorskiy, T. Eralp, M. J. Gladys and G. Held, J. Phys. Chem. C **113** (2009) 21755.

[34] P. Hu and D. A. King, Phys. Rev. B **49** (1994) 2791.

[35] G. Held and H.-P. Steinrück, Surface Sci. **490** (2001) 274.

[36] W. Braun and G. Held, Surf. Sci. **594** (2005) 203.

[37] P. Hu, C. J. Barnes and D. A. King, Phys. Rev. B **45** (1992) 13595.

[38] J. Wang, M. De Angelis, D. Zaikos, M. Setiadi and R. Masel, Surf. Sci. **318** (1994) 307.

[39] G. Held, S. Uremovic, C. Stellwag and D. Menzel, Rev. Sci. Instr. **67** (1996) 378.

[40] G. Held and W. Braun, *CLEED manual*, available from the authors.

[41] J. B. Pendry, *Low Energy Electron Diffraction*, Academic Press, London (1974).

[42] M. A. Van Hove and S. Y. Tong, *Surface Crystallography by LEED*, Springer Series in Solid–State Sciences, Springer, Berlin (1979).

[43] A. Barbieri and M. A. Van Hove, *Phase shift program package*, available from http://electron.lbl.gov/software/software.html.

[44] J. A. Nelder and R. Mead, The Computer Journal **7** (1965) 308.

[45] W. H. Press, B. P. Flannery, S. A. Teukolsky and W. T. Vetterling, *Numerical Recipes in C*, Cambridge University Press, Cambridge (1988).

[46] J. B. Pendry, J. Phys. C: Solid State Phys. **13** (1980) 937.

[47] G. Held, M. P. Bessent, S. Titmuss and D. A. King, J. Chem. Phys. **105** (1996) 11305.

[48] G. Kresse and J. Furthmüller, Phys. Rev. B **54** (1996) 11169.

[49] G. Kresse and D. Joubert, Phys. Rev. B **59**(3) (1999) 1758.

[50] J. P. Perdew, J. A. Chevary, S. H. Vosko, K. A. Jackson, M. R. Pederson, D. J. Singh and C. Fiolhais, Phys. Rev. B **46**(11) (1992) 6671.

[51] P. J. Feibelman, B. Hammer, J. K. Norskov, F. Wangner, M. Scheffler, R. Stumpf, R. Watwe and J. Dumesic, J. Phys. Chem. **105** (2001) 4018.

[52] P. J. Rous, Surf. Sci. **296** (1993) 358.

Coverage	Unit mesh	Atop R_P	Bridge (short) R_P	Bridge (long) R_P
1 ML	$p(2 \times 1)$	0.291 ($\pm$0.04)	0.591 ($\pm$0.09)	0.504 ($\pm$0.09)
0.5 ML	$c(2 \times 2)$	0.222 ($\pm$0.03)	0.346 ($\pm$0.06)	–
0.5 ML	$p(2 \times 1)$	0.222 ($\pm$0.03)	0.311 ($\pm$0.05)	–
0.5 ML	$p(1 \times 2)$	0.220 ($\pm$0.03)	0.304 ($\pm$0.05)	–

Table 1: Lowest R_P factors achieved without optimizing non-geometric parameters for different adsorption sites and models for the 1.0 ML and 0.5 ML structures of CO on Pt{110}.

Pt{111}-$p(2\times1)$-(2CO) ($R_P = 0.242$)					
Atom	rmsd	x ($\parallel$ [001])	y ($\parallel$ [1$\bar{1}$0])	z	
Adsorbate layer					
O	0.19	2.84 ±0.13	-1.47 +0.32/-0.14	6.93 ±0.06	Δx(C-O)=0.39, Δy(C-O)=0.15
O	0.19	1.08	-4.24	6.93	d(C-O)= 1.10, Θ(C-O) = 22° (+3/-9)
C	0.14	2.45 ±0.11	-1.32 +0.25/-0.38	5.91 ±0.06	Δx(C-Pt)=0.55, Δy(C-O)=0.05
C	0.14	1.47	-4.09	5.91	d(Pt-C)=1.85
1st Pt layer					
Pt	0.12	1.90 ±0.18	-1.27 ±0.28	4.14 ±0.06	Δx(vs bulk)=±0.06
Pt	0.12	2.02	-4.04	4.14	Δy(vs bulk)=−0.12
2nd Pt layer					d(1-2)=1.33 (−4%)
Pt	0.07	-0.03 ±0.25	0.06 ±0.18	2.81 ±0.08	
Pt	0.07	0.03	-2.71	2.81	
3rd Pt layer					d(2-3)=1.40 (+1%)
Pt	0.06	1.96	-1.39	1.42 ±0.07	
Pt	0.06	1.96	-4.16	1.42	
4th Pt layer					d(3-4)=1.42 (+2%)
Pt (bulk)	0.06	0.00	0.00	0.00	
					d(bulk)=1.385

Table 2: Atomic coordinates and other relevant parameters for the best-fit geometry of Pt{110}-$p(2\times1)$-(2CO) at 1.0 ML ($R_P =$ 0.242). All coordinates and lengths are given in Å; rmsd = vibrational root mean square displacement, $\Delta x, y$ = lateral displacements, d(C-O)/(C-Pt)=bond length, d(1-2), etc. = vertical inter-layer distances. Some of these parameters are illustrated in Figure 3. The error bars were calculated using Pendry's RR method. They are only indicated for parameters that were optimized and only once for a pair of atoms related by the glide-line symmetry. Note, that inter-layer distances not always match the difference between the z coordinates due to rounding errors. A complete set of coordinates is also supplied in the supporting information.

Atom	rmsd	coordinates			differences			bond lengths / angles
		x (‖ [001])	y (‖ [1$\bar{1}$0])	z				
$p(2 \times 1)$-CO (R_P = 0.170)								
O	0.19	2.24 +17/-24	-1.33 +0.25/-0.36	7.01 ±0.06	Δx(C-O)=0.10	Δy(C-O)=0.08	Δz(C-O)=1.10	d(C-O) = 1.11
C	0.14	2.14 ±0.19	-1.41 ±0.26	5.91 ±0.05				Θ(C-O) = 7°
					Δx(C-Pt)=0.38	Δy(C-Pt)=−0.03	Δz(C-Pt)=1.75	d(C-Pt) = 1.79
1st Pt layer								
Pt	0.12	1.75 ±0.18	-1.38 ±0.27	4.17 ±0.12	Δx(vs bulk)=−0.21	Δy(vs bulk)=+0.01		
Pt	0.12	2.03 ±0.18	-4.11 ±0.20	4.08 ±0.08	Δx(vs bulk)=+0.07	Δy(vs bulk)=+0.04	Δz(buckling)=0.08	
2nd Pt layer							d(1-2)=1.33	(−4 %)
Pt	0.07	-0.06 ±0.28	0.07 ±0.17	2.85 ±0.07				
Pt	0.07	-0.06 ±0.24	-2.73 ±0.18	2.75 ±0.08			Δz(buckling)=0.10	
3rd Pt layer							d(2-3)=1.38	(−0.4 %)
Pt	0.06	1.96	-1.39	1.49 ±0.06				
Pt	0.06	1.96	-4.16	1.35 ±0.09			Δz(buckling)=0.14	
4th Pt layer							d(3-4)=1.42	(+2 %)
Pt(bulk)	0.06	0.00	0.00	0.00				
$c(2 \times 2)$-CO (R_P = 0.183)								
O	0.19	2.28 +0.21/-0.42	-1.61 +0.53/-0.25	7.04 ±0.07	Δx(C-O)=0.11	Δy(C-O)=−0.14	Δz(C-O)=1.10	d(C-O) = 1.12
C	0.14	2.17 ±0.22	-1.48 ±0.26	5.94 ±0.07				Θ(C-O) = 9°
					Δx(C-Pt)=0.31	Δy(C-Pt)=−0.02	Δz(C-Pt)=1.81	d(C-Pt) = 1.84
1st Pt layer								
Pt	0.12	1.86 ±0.28	-1.46 ±0.20	4.12 ±0.12	Δx(vs bulk)=−0.10	Δy(vs bulk)=−0.07		
Pt	0.12	2.07 ±0.23	-4.05 ±0.20	4.12 ±0.09	Δx(vs bulk)=+0.11	Δy(vs bulk)=+0.11	Δz(buckling)=0.01	
2nd Pt layer							d(1-2)=1.29	(−7 %)
Pt	0.07	0.00 ±0.20	0.10 ±0.17	2.85 ±0.06				
Pt	0.07	0.02 ±0.18	-2.84 ±0.25	2.80 ±0.07			Δz(buckling)=0.05	
3rd Pt layer							d(2-3)=1.41	(+2 %)
Pt	0.06	1.96	-1.39	1.47 ±0.12				
Pt	0.06	1.96	-4.16	1.36 ±0.07			Δz(buckling)=0.11	
4th Pt layer							d(3-4)=1.41	(+2 %)
Pt(bulk)	0.06	0.00	0.00	0.00				
$p(1 \times 2)$-CO(R_P = 0.181)								
O	0.19	2.29 +0.17/-0.33	-1.17 +0.23/-0.48	7.01 ±0.07	Δx(C-O)=0.12	Δy(C-O)=0.19	Δz(C-O)=1.09	d(C-O) = 1.11
C	0.14	2.16 ±0.22	-1.35 ±0.27	5.93 ±0.06				Θ(C-O) = 12°
					Δx(C-Pt)=0.33	Δy(C-Pt)=+0.05	Δz(C-Pt)=1.83	d(C-Pt) = 1.85
1st Pt layer								
Pt	0.12	1.84 ±0.20	-1.40 ±0.26	4.10 ±0.12	Δx(vs bulk)=−0.12	Δy(vs bulk)=−0.01		
Pt	0.12	6.07 ±0.17	-1.29 ±0.20	4.11 ±0.09	Δx(vs bulk)=+0.19	Δy(vs bulk)=+0.10	Δz(buckling)=0.01	
2nd Pt layer							d(1-2)=1.29	(−7 %)
Pt	0.07	0.03 ±0.19	-0.13 ±0.27	2.76 ±0.09				
Pt	0.07	3.95 ±0.18	0.09 ±0.14	2.86 ±0.06			Δz(buckling)=0.11	
3rd Pt layer							d(2-3)=1.41	(+2 %)
Pt	0.06	1.96	-1.385	1.45 ±0.12				
Pt	0.06	5.88	-1.385	1.35 ±0.08			Δz(buckling)=0.09	
4th Pt layer							d(3-4)=1.40	(+1 %)
Pt(bulk)	0.06	0.00	0.00	0.00				

Table 3: Atomic coordinates and other relevant parameters for the best-fit geometries of different models for the 0.5 ML layer of CO on Pt{110}: Pt{110}-$p(2\times1)$-CO, Pt{110}-$c(2\times2)$-CO, and Pt{110}-$p(1\times2)$-CO. All coordinates and lengths are given in Å; rmsd = vibrational root mean square displacement, $\Delta x, y$ = lateral displacements, d(C-O)/(C-Pt)=bond length, d(1-2), etc. = vertical inter-layer distances. Some of these parameters are indicated in Figure 6. The error bars were calculated using Pendry's RR method; they are only indicated for parameters that were optimized. A complete set of coordinates for each structure is also supplied in the supporting information.

Average Parameters			
CO	d(C-O) = 1.11 (±0.07) Å	Θ(C-O) = 9° †	
	Δx(C-O) = 0.11 (±0.3) Å	Δy(C-O) = 0.04 (±0.3) Å	Δz(C-O) = 1.10 (±0.07) Å
C-Pt_1	d(C-Pt) = 1.83 ±0.12) Å		
	Δx(C-Pt) = 0.34 (±0.3) Å	Δy(C-Pt) = -0.01 (±0.3) Å	Δz(C-Pt) = 1.80 (±0.12) Å
Pt_1-Pt_2		d(1-2) = 1.30 (±0.12) Å	
Pt_2-Pt_3		d(2-3) = 1.40 (±0.11) Å	
Pt_3-Pt_4		d(3-4) = 1.41 (±0.11) Å	

† See text for a discussion of the error margin of Θ(C-O).

Table 4: Average structural parameters for the 0.5 ML models of CO on Pt{110}. $\Delta x, y$ = lateral displacements, d(C-O)/(C-Pt)=bond length, d(1-2), etc. = vertical inter-layer distances. Some of the parameters are indicated in Figure 6. The error margins given are averages of those for the individual structures.

DFT supercell	$p(2\times1)$		$p(2\times2)$									
Coverage	1.00 ML		0.50 ML								0.25 ML	
Model	(a)		(b)		(c)		(d)		(e)		(f)		(g)	
Molecular arrangement	$p(2\times1)$-2CO		$p(2\times1)$-CO		$p(2\times1)$-CO		$c(2\times2)$-CO		$p(1\times2)$-CO		$p(2\times2)$-2CO		$p(2\times2)$-CO	
Adsorption site	atop	bridge	atop	bridge	atop	bridge	atop	bridge	atop	bridge	atop	bridge	atop	bridge
E_{ad} (eV)	1.921	1.853	2.154	2.074	2.088	2.044	2.040	2.064	1.850	1.808	1.900	1.869	2.087	2.110
d(C-O) (Å)	1.160	1.175	1.160	1.182	1.160	1.179	1.160	1.180	1.159	1.175	1.160	1.178	1.160	1.182
d(C-Pt) (Å)	1.864	2.045	1.857	2.019	1.856	2.025	1.859	2.023	1.865	2.039	1.865	2.039	1.857	2.019
C-O tilt (°)	19	18	6	4	2	2	6	2	6	3	16	20	6	4
Δd(1-2) (%)	−7	+1	−12	−7	−11	−7	−11	−7	−11	−5	−11	−5	−13	−11
Δd(2-3) (%)	0	+3	+4	+7	+4	+7	+5	+7	+4	+5	+4	+5	+6	+7
d(bulk) (Å)	1.411		1.411		1.411		1.411		1.411		1.411		1.411	
ν_{CO}(sym) (cm^{-1})	2073	1937	2054	1878										
ν_{CO}(asym) (cm^{-1})	1997	1858	–	–										
ν_{CO-Pt}(sym) (cm^{-1})	499	423	509	388										
ν_{CO-Pt}(asym) (cm^{-1})	490	374	–	–										

Table 5: Summary of the DFT results. Adsorption energies (per molecule) and structural parameters for different periodicities and adsorption sites of CO adsorbed on unreconstructed Pt{110} at 1.0 ML, 0.5 ML, and 0.25 ML coverages. For the $p(2\times1)$ structures at 0.5 ML and 1.0 ML also frequencies for C-O and C-Pt stretch modes are included in the Table. A complete set of coordinates for each structure is supplied in the supporting information.

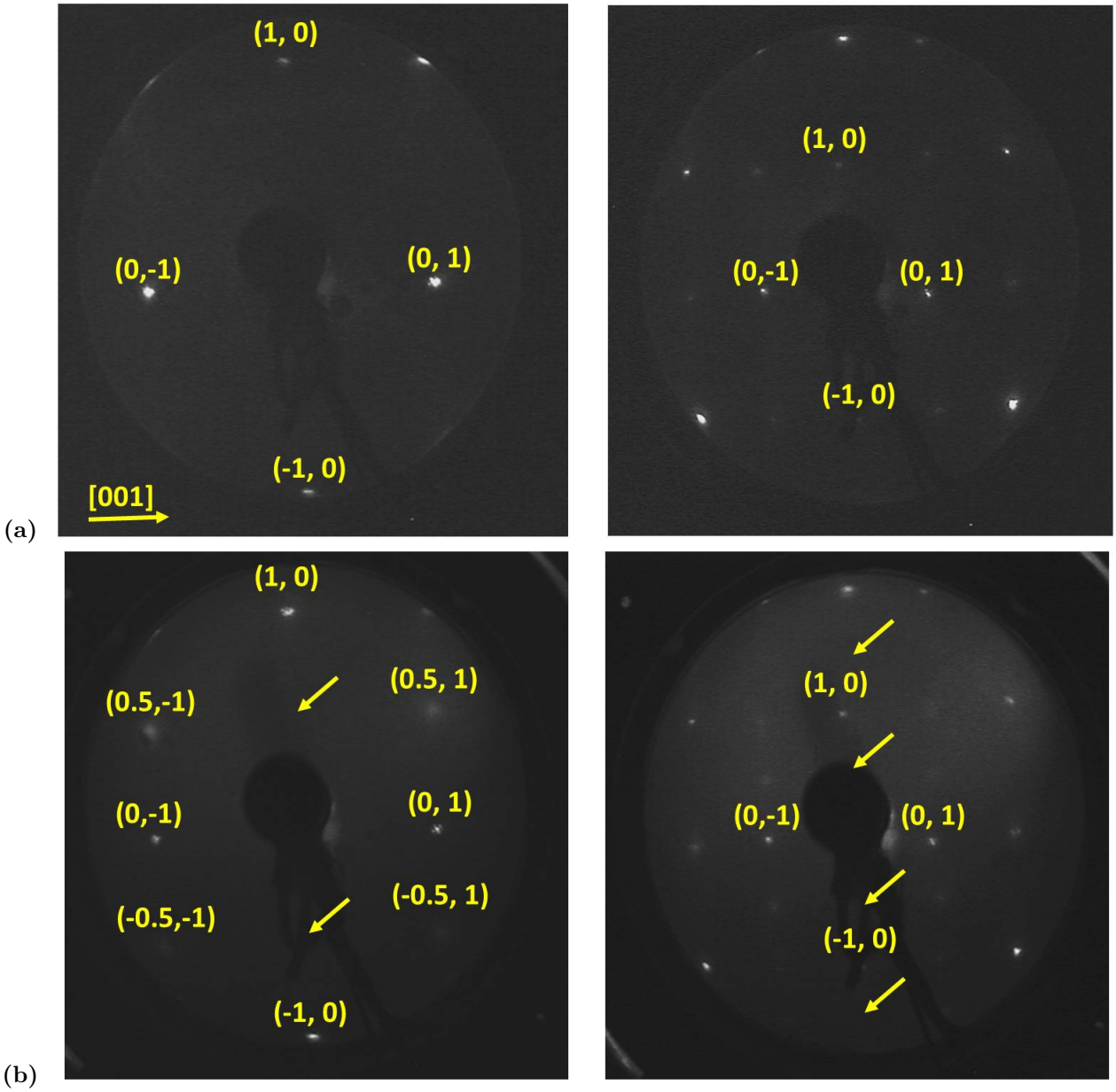

Figure 1: (a) LEED patterns of the disordered Pt{110}-(1x1)-0.5 ML CO phase at 50 eV (left) and 150 eV (right) at sample temperature 100 K. (b) LEED patterns observed for the Pt{110}-$p(2 \times 1)$ phase (CO saturation coverage) at 50 eV (left) and 150 eV (right). The absence of the $(\pm(h + \frac{1}{2}), 0)$ spots (indicated by arrows) indicates a glide line in the $[1\bar{1}0]$ direction. Indices are included for the first-order integer spots and some of the superstructure spots (on the left of (b))

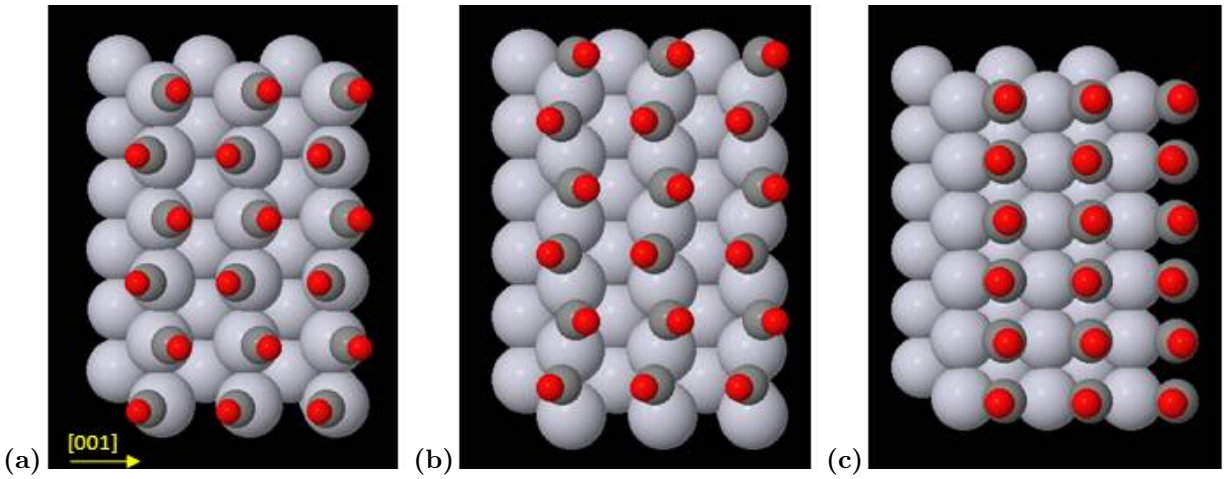

Figure 2: Schematic top view of the Pt{110}-$p(2 \times 1)$-(2CO) trial structures for 1.0 ML coverage: (a) atop, (b) short bridge and (c) long bridge adsorption sites.

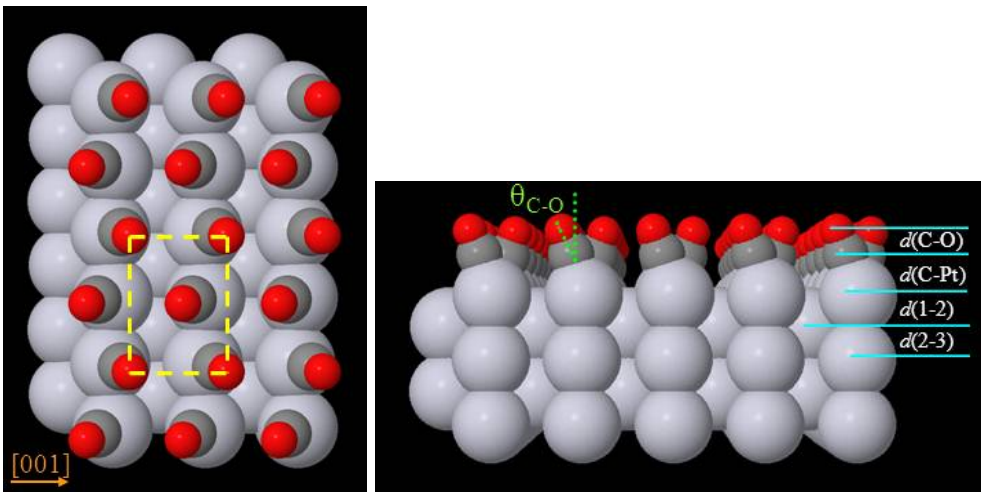

Figure 3: Schematic top view (left) and side view (right) of the best-fit LEED structure for Pt110-$p(2\times1)$-(2CO) at 1.0 ML. See text for details.

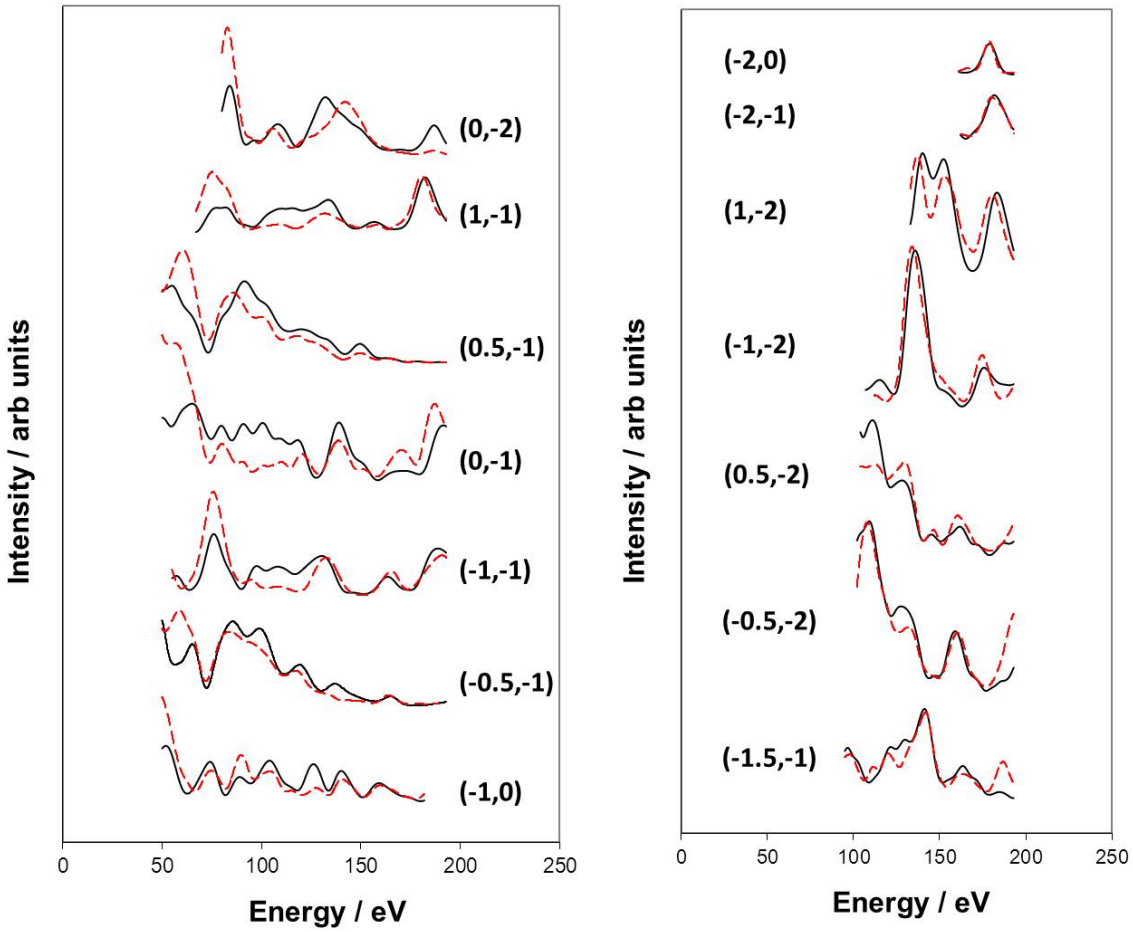

Figure 4: Experimental (black) and theoretical (red) IV curves for all individual beams of the best-fit Pt110-$p(2 \times 1)$-(2CO) structure. The total R_P value for this model is 0.242.

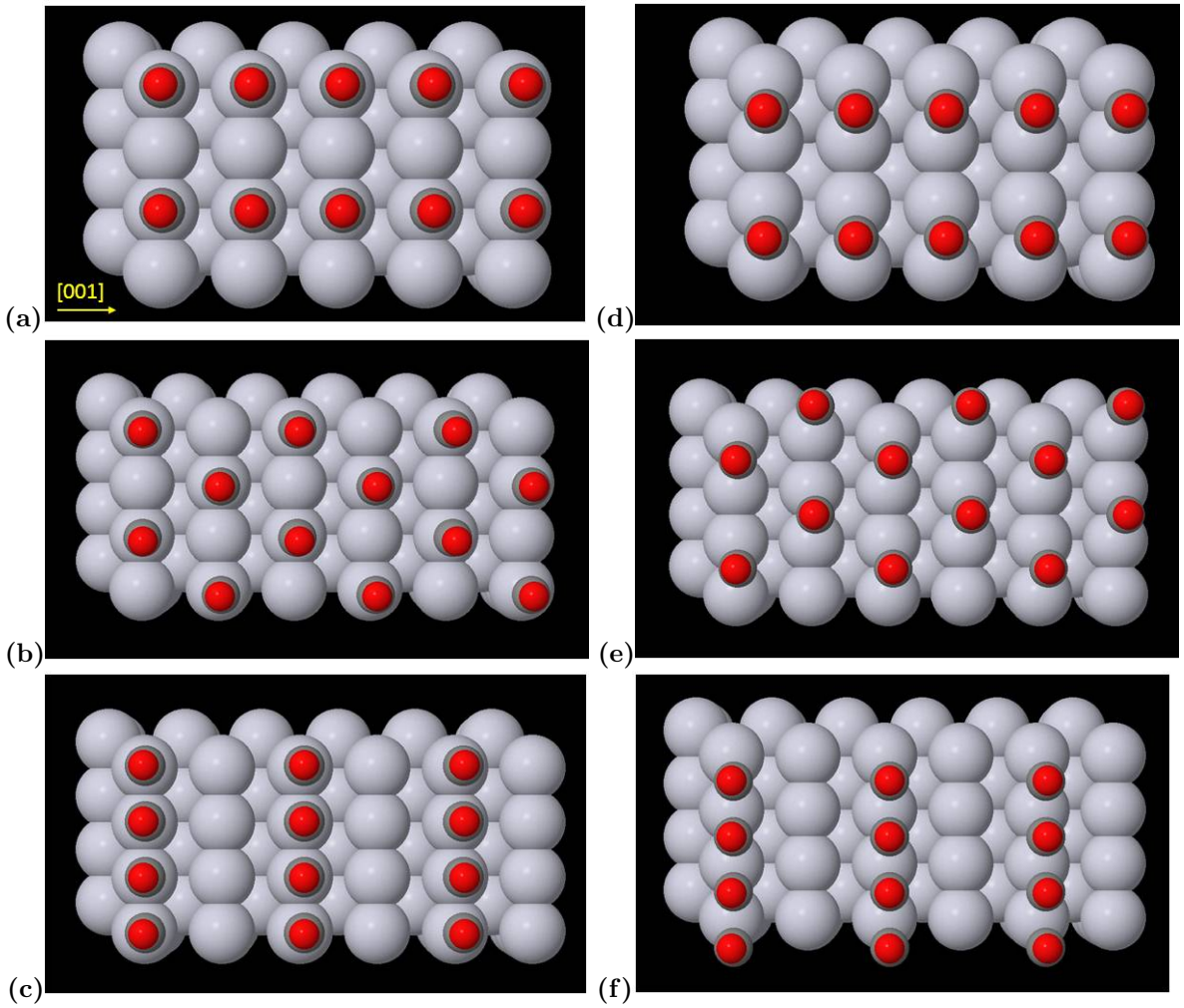

Figure 5: Schematic top view of the trial structures for 0.5 ML CO on Pt{110} with atop (a)-(c) and bridge (d)-(f) adsorption sites: (a,d) $p(2 \times 1)$, (b,e) $c(2 \times 2)$ and (c,f) $p(1 \times 2)$ unit mesh.

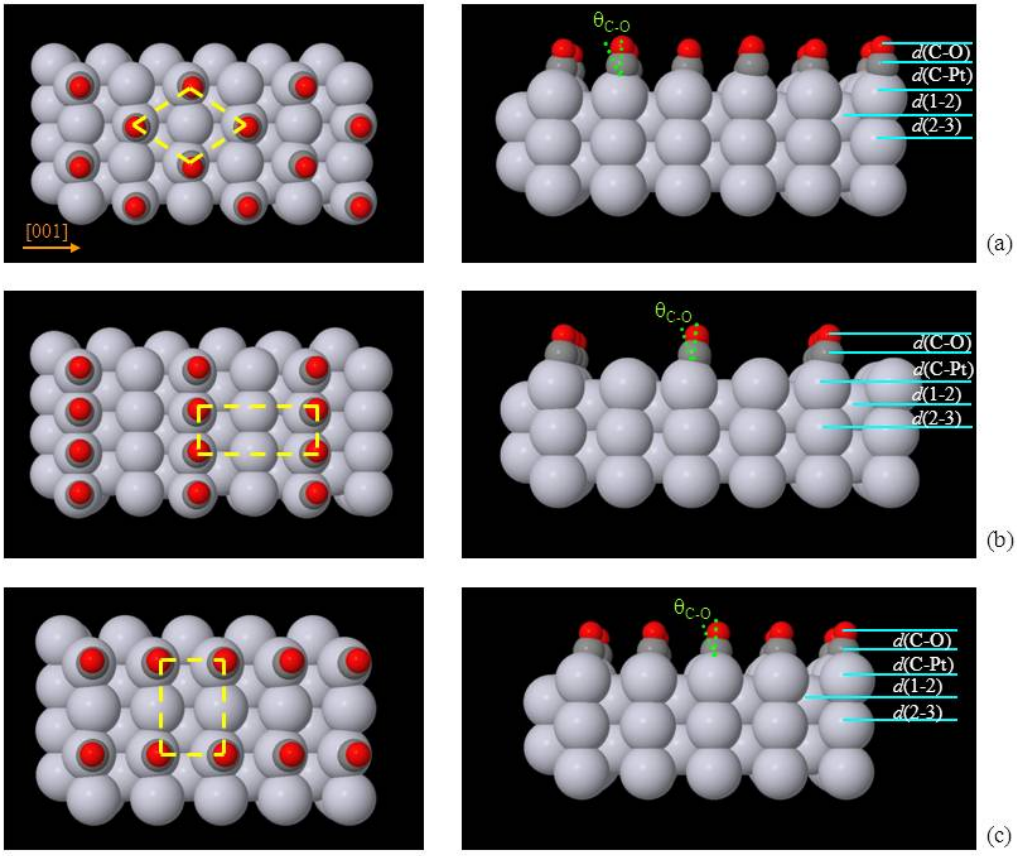

Figure 6: Schematic top view (left) and side view (right) of the best-fit surface geometries for 0.5 ML CO on Pt{110}:(a) $c(2 \times 2)$, (b) $p(1 \times 2)$ and (c) $p(2 \times 1)$. The yellow dashed lines in the left images indicate the unit mesh. See text for further explanation.

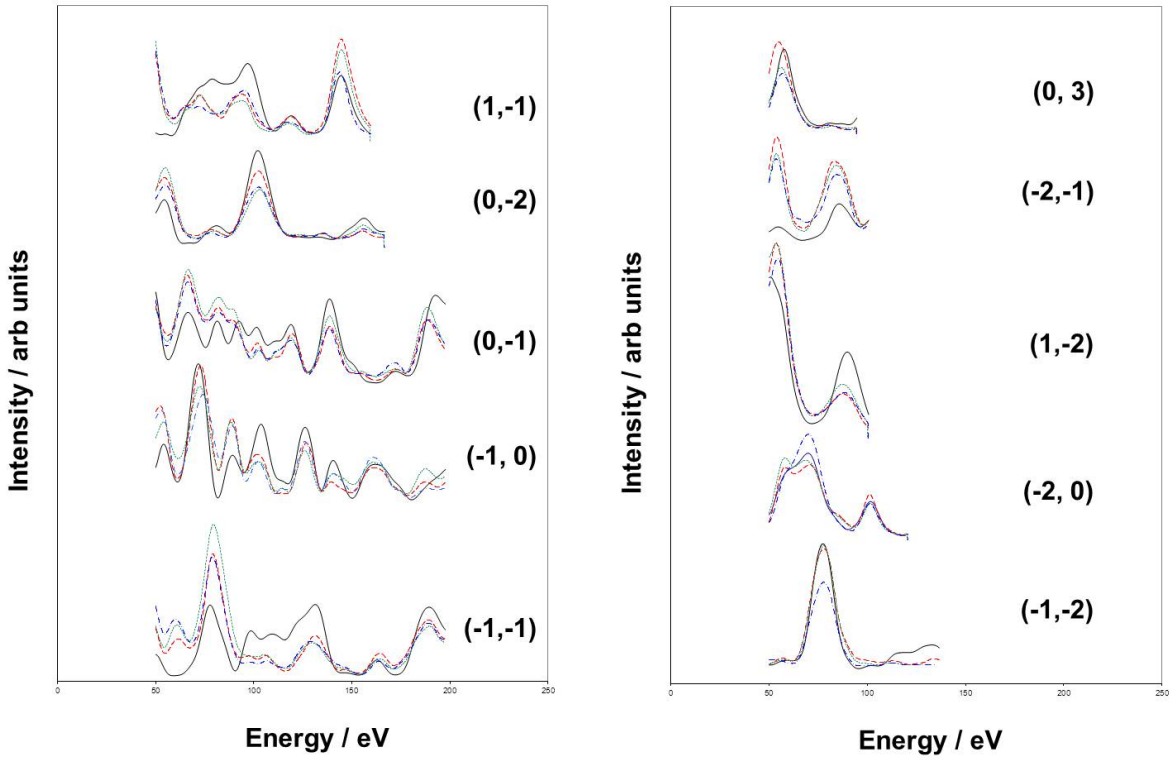

Figure 7: Experimental (black) and theoretical IV curves for the $c(2 \times 2)$ (red), $p(2 \times 1)$ (green) and $p(1 \times 2)$ (blue) structures modeling the disordered CO layer at 0.5 ML coverage.

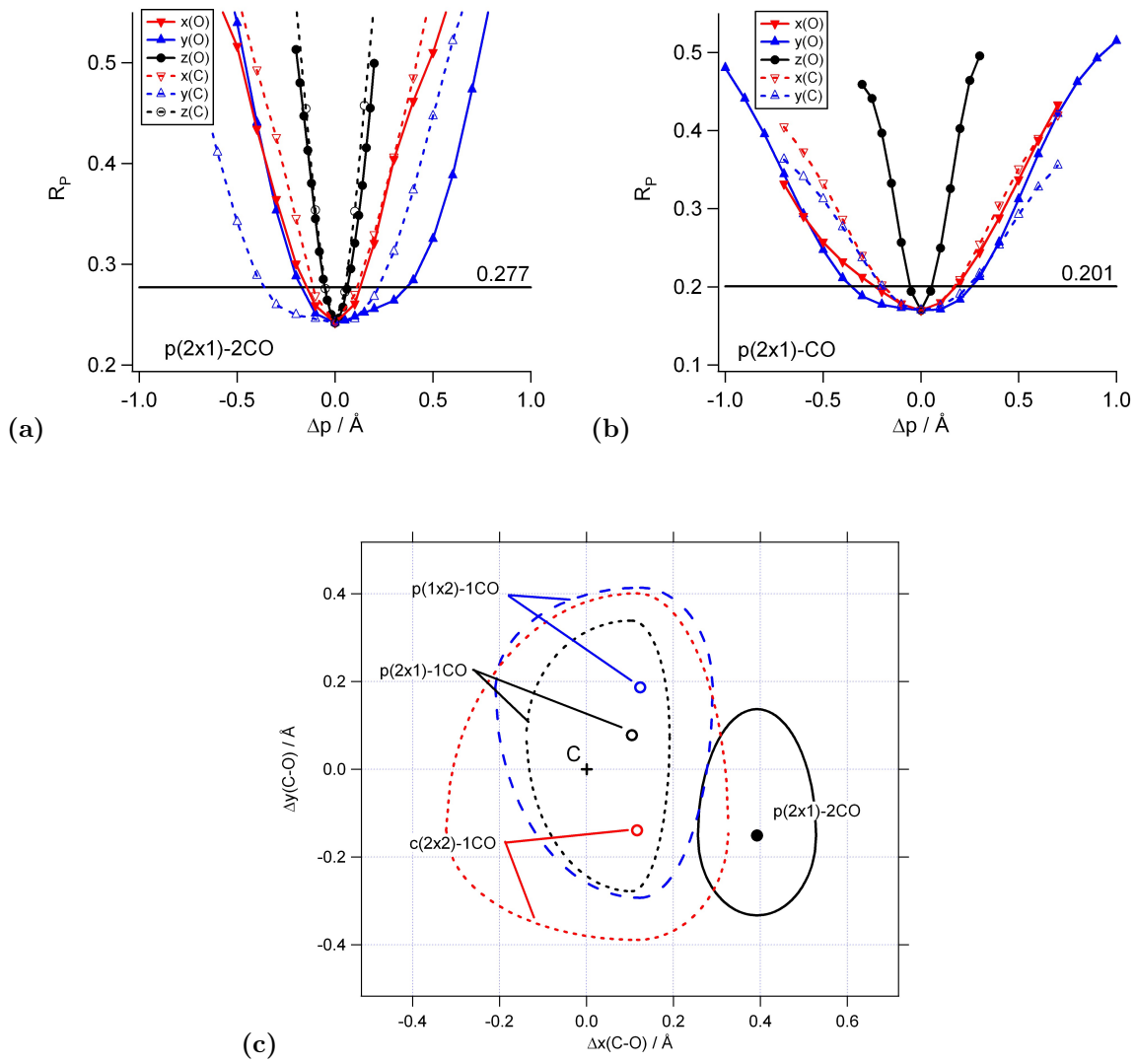

Figure 8: (a,b) Plots of R_P factors vs displacements of O (filled symbols) and C coordinates (open symbols) from their best-fit values for the $p(2 \times 1)$-(2CO) (a, 1 ML) and $p(2 \times 1)$-(CO) (b, 0.5 ML) structures. The horizontal lines at $R_P = 0.277$ and 0.201, respectively, mark the upper limit of the statistical error margin of R_P, $R_{min} \cdot (1 + RR)$.

(c) Error ranges of x and y displacements of the oxygen atom with respect to the underlying carbon atom for the four models tested. The x/y position of the carbon atom is marked by a cross at (0,0); the best fit positions of the oxygen atoms are marked by open circles for the 0.5 ML models and a filled circle for the $p(2 \times 1)$-(2CO) 1 ML model. The error boundaries in the two-dimensional plot were interpolated between the one-dimensional boundaries using elliptical splines. An upright orientation of the CO molecule is clearly outside the error range for the 1 ML structure, whereas the error ranges of the 0.5 ML structures are all centered near the upright position.